_____

THEMATIC ISSUE

Simulating seismic chimney structures as potential vertical migration pathways for CO_2 in the Snøhvit area, SW Barents Sea: model challenges and outcomes

Alexandros Tasianas · Lena Mahl · Melanie Darcis · Stefan Buenz · Holger Class

Abstract Carbon Capture and Storage (CCS) activities at the Snøhvit field, Barents Sea, will involve carrying out an analysis to determine which parameters affect the migration process of CO_2 from the gas reservoir, to what degree they do so and how sensitive these parameters are to any changes. This analysis will aim to evaluate the effects of applying a broad but realistic range of reservoir, fault and gas chimney properties on potential CO_2 leakage at various depths throughout the subsurface. Fluid flow might take place through parts of or the entire extent of the overburden. One of the aims of the analysis is assessing the potential of CO_2 reaching the seabed. Using the Snøhvit gas reservoir and overburden in the Barents Sea, a series of geological models were built using seismic and well-log data. We then performed numerical simulations of CO_2 migration in focused fluid flow structures. Identification of potential migration pathways and their extent, such as gas chimneys and faults, and their incorporation into these models and simulations will provide a realistic insight into the migration potential of CO_2. In the simulations the CO_2 is injected over a 20 year period at a rate of 0.7 Mt/year and migration is allowed to take place over a 2000 year time frame for domains of approximately 21 Km^2 for the caprock fault models, 24 Km^2 for the realistic gas chimney models and 35 Km^2 for the generic gas chimney models, in a layered sedimentary succession. The total mass of CO_2 injected in the reservoir during the 20-year injection period is 14 Mt. There is a strong interaction between the various parameters but the parameter that had the most influence on the CO_2 migration process was probably the permeability of the reservoirs, especially the average permeability (k). Also, for the faulted caprock scenarios, it should be noted that at near surface depths the permeability of 765 mD is already adequate for a good CO_2 flow. At the chimney top level (600 m) however, a further increase in permeability has an additional effect on improving CO_2 flow. Overall, considering the slow upward migration velocity of the plume, this geological setup can be regarded as a suitable storage site.

A. Tasianas (✉) · S. Buenz
CAGE - Centre for Arctic Gas Hydrate, Environment and Climate, Department of Geology, UiT The Arctic University of Norway, Tromsø, Norway
e-mail: alexandros.tasianas@uit.no
Tel : +47 90978038

L. Mahl · M. Darcis · H. Class
Dept. of Hydromechanics and Modeling of Hydrosystems, University of Stuttgart, Stuttgart, Germany

Introduction

This paper deals with the simulation of fluid flow in the greater Snøhvit area in the SW Barents Sea, comprising several hydrocarbon discoveries, the Snøhvit, Askeladd and Albatross fields (Figure 1)(Hansen and Rasen 2012). Gas production at Snøhvit started in 2007 and CO_2 capture in 2008 (Hansen and Rasen 2012). The gas production system feeds gas into the Snøhvit Liquefied Natural Gas processing plant on Melkøya Island near Hammerfest in Northern Norway. The plant emits 920,000 tons of CO_2 each year (Linjordet and Olsen 1992).

The CO_2 injection point (Figure 2) is located in the Tubåen Formation (at 2560-2670 m depth below the sea surface); a mostly sandy reservoir (Hansen et al. 2011) and the main CO_2 storage formation in the area. At this depth, the hydrostatic pressure exceeds 280 bar and the temperature reaches roughly 80 °C (Eiken et al. 2011).

The oil produced from Snøhvit is from the first offshore oil field, which corresponds also to a major CO_2 storage opportunity (Edlmann et al. 2015), where oil is produced without using offshore installations. Statoil is the operator of the CO_2 storage at Snøhvit. CO_2 is removed from the gas stream and piped 150 km back to the field for injection into an offshore deep saline formation. The main CO_2 storage formation is the Saline Tubåen Sandstone Formation; a reservoir located at 2600 meters depth. In early 2010 Statoil announced that they had discovered that there was less storage capacity than expected at the Snohvit injection site. As of late 2011, injection has subsequently changed to the lower parts

of the Stø Formation. Around 700,000 tonnes of carbon dioxide per year will be stored in this way. A monitoring program has also been set-up to investigate the behaviour of CO_2 underground (Schutze et al. 2012).

Several large leakage structures, so-called gas chimneys, occur in close vicinity to the Snøhvit field (Ostanin et al., 2013). These leakage structures are potentially related to the denudation and uplift history of the Barents Sea region which likely led to the spilling of reservoirs (Makurat et al. 1992; Rodrigues Duran et al. 2013). However, the exact mechanisms and timescales of leakage are poorly understood. But any risk assessment for CO_2 storage would need to consider what impact these gas chimneys have on the storage operation.

The aim of this study is to carry out numerical simulations on various parameters related to the gas chimneys that are found in the overburden at Snøhvit (Figure 2). These gas chimneys, which have been interpreted and mapped on the seismic data, correspond to wide zones of deteriorated seismic signal, probably associated with low velocity zones caused by shallow gas accumulations or vertical gas migration (Loseth et al. 2009). The developed fault network, characterizing the Snøhvit field, will also be interpreted from the available seismic data and studied further by running various numerical simulations based on different scenarios. There are three groups of scenarios: 1) faulted caprock scenarios 2) realistic gas chimney scenarios and 3) generic gas chimney scenarios.

Potential CO_2 flow along existing wells, coupled with faulted stratigraphic sequences, missing well logs that need to be computed, thus providing highly uncertain parameters, makes modeling challenging. The quantitative analysis of the risk of CO_2 migration is an important computational challenge itself and the pathways that the migrating fluid can take is an important variable. The chosen "leakage" scenarios are purely hypothetical and use preexisting fluid flow pathways, such as gas chimneys and faults, identified in the Snøhvit area. These structures have been created in the past by fluid migration and tectonic activity. They have not been formed recently due to CO_2 sequestration. The values of maximum flux rates reached under certain conditions and the type of gas chimney permeability that is critical for avoiding that CO_2 reaches the seabed could be thus determined. To decide on the importance of these parameters, all of the statistical data were cross-plotted as shown in the results section below.

Geological setting and study area

The Snøhvit gas field is located in the Barents Sea (Figure 1a), in the central part of the Hammerfest Basin at a water depth of 310 - 340 m and at about 160 km from the coastline of Northern Norway (Figure 1b) (Hansen and Rasen 2012).

The Barents Sea is part of the Arctic Ocean located north of Norway and Russia. It is bordered by Novaya Zemlya in the east, Franz Josef Land and Svalbard in the north and the Norwegian Sea in the west. With an area of 1.3 million kms² and water depths averaging approximately 300 m, it is one of the largest areas of continental shelf in the world.

The Barents Sea shelf can be divided into a series of basins and highs with the SW Barents Sea being characterized by relatively deep sedimentary basins. These basins have undergone several episodes of crustal extension and basin formation from Late Paleozoic to Early Tertiary (Faleide et al. 2008). The western part of the Barents sea shelf is dominated by a system of NNW-SSE and N-S striking structural features, while ENE-WSW striking fault complexes have dominated the central and eastern parts (Faleide et al. 2008).

The ENE-WSW oriented Hammerfest Basin, located in the SW Barents Sea, was probably established in the Late Carboniferous (Gabrielsen et al. 1990), with important subsidence events in the Triassic and Early Cretaceous and with the main basin development phases taking place during the Mid to Upper Jurassic times (Linjordet and Olsen 1992).

At Snøhvit, the Stø Formation is the main reservoir rock in the Hammerfest Basin, of Pliensbach-Bajocian age, consisting of vertically stacked units of the lower to the upper beach slope deposits (Worsley et al. 1988). CO_2 has been injected into the Tubåen Formation, of Lower Jurassic age, since 2008 (Maldal and Tappel 2004). CO_2 storage was changed from the Tubåen Formation to the lower part of the Stø Formation in March 2011 (Moumets et al. 2015).

Geological model and "leakage" scenarios
Geological zones

For the analysis, geological models need to be built (Norden et al. 2012), based on interpreted 3D conventional seismic data from a data set, namely (ST0306), provided by Statoil. The water depth in the Snøhvit and Albatross fields in the Hammerfest Basin, ranges from 315 m to 355 m (Figure 1). It was collected in 2003 by the seismic company PGS for Statoil. Schlumberger Petrel software was used to interpret the seismic data, locate the various geological features, such as the gas chimneys and the faults, integrate well-log information and build the geological models.

The analysis is applied to a realistic geological system related to the Snøhvit field which has a wealth of seismic and well log data to build proper geological models. The geological models consist of a deep saline aquifer, the Stø Formation, overlain by the Hekkingen Formation caprock and overburden formations. Using established stratigraphy (Worsley et al. 1988) and well-log correlation all the major stratigraphic units in the Snøhvit area were identified. Formation tops were interpreted throughout the whole survey but for the purposes of fluid flow modeling the main focus was on areas around the Snøhvit reservoir. For the outline and location of the generic and realistic gas chimney and caprock fault model, see Figure 2. Altogether 10 surfaces were mapped, from the seabed down to the Top Snadd reflector. The surfaces that were used in the modeling are the seabed, the Upper Regional Unconformity, the top Kviting, the Intra Kviting, the top Kolje, the top Knurr, the top Hekkingen, the top Fuglen, the top Tubåen and the top Fruholmen. These 10 surfaces, were used as an input for building the geological models, resulting in models with 9 zones which, were then filled with petrophysical property values such as porosity (φ) and permeability (k).

Parameters such as average permeability, fault permeability and fault thickness for the caprock fault scenarios were then varied. In the gas chimney models, either realistic or generic, the parameters that were varied

correspond to the chimney permeability, chimney width, and number of chimneys and the permeability of zone 9.

It should be noted that the "average permeability" in the models corresponds to the estimated permeability for the rocks found outside the above-mentioned specific geological objects, such as zone 9 of the reservoir, faults and gas chimneys. The permeability in these last-mentioned geological objects is described by a different permeability distribution, either derived from literature or experimentally, and is referred to as "chimney permeability" in the case of gas chimneys for example, or "zone 9 permeability" for the permeability of a part of the reservoir.

Fault, chimney or zone 9 permeability thus refers to the permeability within these geological objects or layers, which remains constant throughout the object for each scenario. Fault thickness refers to the thickness of the fault zone in the model, which is characterized by a different permeability than the surrounding rock. Chimney width refers to the diameter of the cylinder describing the generic gas chimneys. The number of generic gas chimneys is varied between 1 and 2.

Varying average permeability, permeability of zone 9 (corresponding to the Tubåen reservoir in the models), and chimney permeability, or the number and width of gas chimneys for the gas chimney scenarios, generic or realistic (Figure 3) will permit to get a better idea of the influence of each parameter variation on the migration process and the corresponding time frame. This will determine whether there is a need to know the permeability of the chimney or fault, for example, whether it is necessary to drill into it and how important a certain parameter is for the CO_2 migration assessment.

Near the main reservoir and the CO_2 injection site, well data is generally too sparse. Obtaining reliable and valid geological models is thus challenging due to the uncertainty in the petrophysical values assigned to individual sedimentary formations. Once these values obtained, they would provide robust input for the fluid-flow modeling; an input which was obtained by using proxy data.

The exploration well that was drilled into gas chimneys in the Ulleung Basin of the East Sea (Kim et al. 2011), provided reliable porosity and permeability values for the large gas chimney structures at Snøhvit (Table 1 annex); also used for this analysis.

CO_2 migration was modeled using a multiphase system, which means that pre-existing fluids within each flow path may have significant impact on the fluid migration.

In order to take into account the uncertainty of the parameterisation of the geological models, we chose to create three different geological models, i.e. a *HIGH*, a *MEDIUM* and a *LOW* case. These cases are characterized by permeability and porosity values in the high, the medium and the low range of available data, (Table 1 in annex). This uncertainty range is based on calculating standard deviations for both porosity and permeability from the analyzed well logs for each identified zone. For more information on the methodology used and the results derived, its essential to consult the "ECO2 project MS12 Geological models report" (Buenz et al. 2012). See also the following web link, http://www.eco2-project.eu/home.html, for accessing various other related ECO2 project reports.

In all permeability models, the caprock (zone 7) permeability is assumed at 10 nD. The permeability of shale is often in the nano-Darcy scale or even lower (Figures 3a and 3b). The caprock is composed of shale layers (Maldal and Tappel 2004) and due to the low permeability of compacted clays, shale zones can easily become overpressured (Chenevert and Sharma 1991; Katsube et al. 1991; Van Oort et al. 1996).

Here, the term "overpressured" refers to the initial condition of clays or shale zones before CO_2 injection. Overpressure can be caused, within the pore space, by (charging) fluid expansion mechanisms, such as expulsion/ expansion of intergranular water during clay diagenesis. Here, overpressure results when the rock matrix constrains the pore fluid as the fluid tries to increase in volume (Opara 2011). The change of pore pressure in clays and shale zones will be minimized. The low permeability that characterizes these shale zones and clays will as a result prevent pressure diffusion or fluid flow.

Fluid flow structures

Based on the 9 zone model, three different model types for investigation of the CO_2 migration potential were defined (Figure 3).

In the modeling, it was assumed that these preexisting fluid flow structures can be reactivated and be used by the injected, upward migrating CO_2 as potential pathways for CO_2 leakage.

Before discussing the simulation results, based on the various sensitivity scenarios, it is essential to clarify the driving force for CO_2 migration which varies depending on injection operations. Advection will be the main driving force during injection; with gravity forces tending to redistribute the injected CO_2. After the end of the injection operation, when injection stops, the pressure gradients will eventually decrease and buoyancy-driven natural convection will become the major driving force. Injected CO_2 dissolves into formation brines from above, increasing brine density and creating an unstable hydrodynamic state favorable for natural convection (Ouakad and Nasrabadi 2012). For buoyancy-driven flow, the properties of geological structures and fluids will play a significant role in determining the fate of CO_2 leakage. Buoyancy-driven advection and convection will also accelerate the dissolution of the CO_2 hydrate and the downward transport of CO_2 (House et al. 2006).

Realistic faults model

Faults represent areas of weakness and in the study area both permeable and impermeable faults are found (Løtveit et al. 2012; Ostanin et al. 2013; Ostanin et al. 2012). Faults were interpreted and mapped throughout the extent of the 3D seismic space and also in depth throughout the overburden, caprock and reservoir. Typical permeabilities are in the range of (0.00001 – 0.0001 mD) for low permeable fault zones and (0.001 – 10 mD) for highly permeable damage zones (Mizoguchi et al. 2008; Moore et al. 2009). Due to a lack of fault permeability and thickness data for the Snøhvit area, a fault permeability, based on the work of Mizoguchi, Hirose et al. 2008 and Moore, Lockner et al. 2009, ranging over (0,0001, 1, 50, 100 and 300 mD) (Figure 3a) was used for the

simulations concerning the Snøhvit case. In these simulations two fault thicknesses were used (50 m and 150 m) based on real fault thicknesses characterising fault zones around the world (Handy et al. 2007; Wibberley and Shipton 2010).

The porosity is not varied in this study. For the average porosity, the values for the MEDIUM scenario (see Annex, table 1) with a fault porosity of 18% are applied. 18% is the maximum value found in a core from the San Andreas Fault (Janssen et al. 2011).

Regarding the porosity parameter, it is important to note that larger porosity reduces the maximum overpressure. For the propagation of the overpressure pulse we have (r $\propto \sqrt{Dt}$), where the hydraulic diffusivity D, (D = k / $\mu c_t \varphi$), is reversely proportional to porosity (φ). This signifies that larger porosity causes shorter propagation of the pressure pulse and reduces the maximum overpressure, since the propagation of the overpressure pulse depends on porosity. Thus, in the case of larger porosity, the same amount of CO_2 occupies a smaller region of the aquifer, hence retarding the attenuation of this pulse (Gonzalez-Nicolas et al. 2012).

The shape of the plume also depends on porosity and lower porosity results in faster plume propagation and a higher likelihood of encountering "leaky" pathways (Gonzalez-Nicolas et al. 2012). This is because smaller porosity is expected to result in larger "leakage" rates (Gonzalez-Nicolas et al. 2012).

Realistic gas chimney model

Gas chimneys correspond to major fluid flow pathways and can be promoted by a connected fracture network penetrating the reservoir's caprock (Arntsen et al. 2007; Ligtenberg 2005; Meldahl et al. 2001).

The realistic gas chimney scenarios are based on existing gas chimneys that were identified and mapped by interpreting 3D conventional seismic data from the (ST0306) data set in the Snøhvit area (Ostanin et al. 2013; Ostanin et al. 2012). The gas chimneys were identified by locating the areas characterized by low amplitude chaotic seismic reflections in the data set.

The modeled gas chimney permeability values used range from 342 to 765 to 3000 mD according to the case, either Low, Medium or High, used (Figure 3b, Table 1). All above values fall within the range observed in gas chimneys in the Ulleung basin, East Sea (Kim et al. 2011), but also applied in this context. The permeability of zone 9 in the models, is varied from 130 to 500 to 880 mD according to the case used (Table 1 in annex). The average permeability (excluding zone 9) is also varied according to the case used (Figure 3b, Table 1 in annex). The porosity is set constant to the values for the Medium scenario. The above range of permeability values, within zone 9 of the reservoir and outside of it, have been calculated in previous studies (Buenz et al. 2012) and correspond to experimental data or data from literature associated with the Snøhvit area.

To determine which property values to use for gas chimney modeling, a reference is made to the study by (Kim et al. 2011), which shows a slight gradual decrease of porosity (from density logs) with depth within the chimney (for UBGH1-9 well from 74.6% - 63.7% and for UBGH1-10 well from 83.3% - 70.6%). From the above values, an average porosity of 71.33% was used for modeling and was assumed constant with depth (Table 1)(Kim et al. 2011).

Table 1. Porosity and permeability estimates used in the 3 scenarios of the realistic gas chimney model

Scenario	Porosity (%)	Permeability	
		Horizontal (D)	Vertical (mD)
Low	63.7	0.46	342
Medium	71.3	1.03	765
High	83.3	4.84	3350

Generic gas chimney model

Building generic models is required since it is not possible to run simulations concerning all relevant geological features, processes and events in the storage complex of the study area. It's also difficult to consider the multitude of seepage-related structures in the overburden and at the seabed with currently available reservoir modeling software.

Generic chimney simulation studies are important as they provide a lot of new information. First of all, they model idealized simple geometries with free parameterisation which allows us to better understand the importance of each of the parameters on the leakage process. Secondly, the storage of CO_2 may create focused fluid flow structures due to blowout events. The generic chimney simulations thus aim to simulate the flow along such structures, but not the process of formation. For this purpose, generic chimneys were placed in the direct vicinity of the injection point to measure the near-field effect of high permeable fluid conduits. The generic chimneys are characterized by a cylindrical shape, a theoretical location and are designed to penetrate through the entire subsurface that is modeled in the generic gas chimney models.

In these scenarios, the same geological background as in the fault models is applied. The CO_2 is injected at the location of the real injection site (Figure 3c). The models have been designed to contain either one or two cylindrical generic gas chimneys, 1 km away from the real injection site either to the north and/or to the south of it (Figures 2 and 3c). Besides the average permeability (Low, Medium, High) (Table 1 in annex), the chimney permeability (342, 765 to 3000 mD), and the chimney width (200, 400 to 600 m) are varied (Figure 3c). Although this gas chimney width range is based on hypothetical values, it corresponds to realistic dimensions of the gas chimneys in submarine sediments worldwide (Cartwright et al. 2007; Cathles et al. 2010). For both the chimneys and the rest of the model the Medium scenario average porosity values were used (Table 1 in annex).

Model dimensions

Table 2 below shows the 9 zones of the geological models and the number of layers included in the simulation grids (Figures 3b and 3c). The faulted models contain only 4 zones (the caprock, one zone above and the 2 reservoir zones below the caprock) (Figure 3a). The overburden in the new grids of the realistic fault models that were built was ignored. The flux

was measured only at 2300 m depth, corresponding to the top of the caprock.

Table 2. Number of layers contained in each zone of the models for the 3 model types

Zone	Number of layers		
	Realistic fault model	Realistic gas chimney model	Generic gas chimney model
1		2	2
2	not applicable	8	8
3		2	2
4		10	10
5		5	5
6	3	2	2
7	4	3	3
8	10	7	7
9	11	10	10
Total	28	49	49

The faulted caprock geological model covers an area of 21.1 Km^2, reaches -2771 m in depth (Figure 3a, Table 3) and its cell resolution in the horizontal plane is 25 m by 25 m and 17.68 m in the vertical plane.

The realistic gas chimney geological model covers an area of 23.7 Km^2, reaches -3025 m in depth (Figure 3b, Table 3), with a cell resolution in the horizontal plane of 50 m by 50 m, which remains quite constant throughout the whole model domain (Table 3). The vertical resolution varies quite strongly due to the layered geology characterising the study area but has an average of 49.87 m (Table 3). The generic gas chimney geological model covers an area of 35.4 Km^2, reaches -2804 m in depth (Figure 3c, Table 3) and has a cell resolution in the horizontal plane of 50 m by 50 m and 48.15 m in the vertical plane (Table 3).

Table 3. Summary of main characteristics for each model type

Characteristics	Fault Model	Realistic Gas chimney Model	Generic Gas chimney model
Domain X width (m)	5275	3950	5950
Domain Y width (m)	4000	6000	5950
Elevation depth range (m)	from -2771 to -2028	from -3025 to -318	from -2804 to -310
Grid cells (nI×nJ×nGrid layers)	211×160×28	120×79×49	119×119×49
Number of iconized horizons	5	10	10
Average Xinc (m)	25	50	50
Average Yinc (m)	25	50	50
Average Zinc (m) (along pillar)	17.68	49.87	48.15

Considered Scenarios

Tables 4, 5, 6 illustrate the different combinations of parameters for each of the three model types.

Table 4: Faulted caprock scenarios description

Scenario	Average permeability	Fault Thickness (m)	Fault permeability (mD)
F1	Medium	50	50
F2			1
F3			100
F4			300
F5		150	50
F6			100
F7			300
F8	Low	50	50
F9			100
F10			300
F11		150	50
F12			100
F13			300
F14	High	50	50
F15			100
F16			300
F17		150	50
F18			100
F19			300

Table 5: Realistic gas chimney scenario description (closed reservoir to avoid "leakage" at boundaries)

Scenario	Average permeability	Chimney permeability (mD)	Zone 9 permeability (mD)
C1	Medium	765	500
C2		342	
C3		3000	
C4		765	130
C5			880
C6	Low	765	500
C7		342	
C8		3000	
C9		765	130
C10			880
C11		342	130
C12			880
C13			130

C14		3000	*880*
C15	**High**	765	*500*
C16		342	
C17		3000	

Table 6: List of generic gas chimney scenarios, with either 1 or 2 chimneys (the reservoir is left open; the square domain is sufficient for preventing CO_2 reaching the boundaries)

Scenario	Average permeability	Chimney permeability (mD)	Chimney width (m)
G1	**Medium**	765	*200*
G2			*400*
G3			*600*
G4	**Low**		*200*
G5			*400*
G6			*600*
G7	**High**		*200*
G8			*400*
G9			*600*

Simulation model and framework conditions

Multiphase-multicomponent flow and transport processes (Helmig 1997) in porous media are modeled using the numerical simulator software DuMuX (Flemisch et al. 2011). It is based on the Distributed and Unified Numerics Environment (Bastian et al. 2006). Depending on the phase-component composition, different standard models are available. The properties for modeling a CO_2 and brine system are described in (Bielinski 2006; Darcis 2012).

In order to account for dissolution, two-phase two-component (2p2c) models need to be set up. The resulting high grid resolution will lead to an overestimation of the dissolved CO_2 in the cells and thus the CO_2 escape will be underestimated, due to numerical dispersion.

The manifestation of a numerical dispersion is related to the finite size of the numerical grid blocks at the interface between the invading CO_2 front and the resident brine. There is an overestimation of the amount of CO_2 that has dissolved into the brine and the error that arises is due to the instantaneous equilibrium between phases that is assumed in each computational cell (Green and Ennis-King 2012).

For our simulations a two-phase (2p) model was used. It neglects the dissolution process, the mutual solubility of CO_2 and H_2O and the transport of the dissolved components in the fluid phases. The 2p model will create a CO_2 plume that is larger and overestimate CO_2 escape and risk whilst computing faster and providing a more conservative estimate.

The main difference between the 2p model approach, used in this piece of work, and general flow and transport simulations is the absence of different components, soluble in one another. This corresponds to an absence of dissolution and diffusion processes, as mentioned above. This method is justified as neglecting dissolution processes results in a systematic overestimation of the free CO_2 and the transport velocities. As explained before, CO_2 that dissolves in the surrounding brine increases the brine density which results in a downwards migration of the CO_2-rich brine. This effect prevents upwards migration of the dissolved CO_2. The resulting conservative estimates of CO_2 leakage using the 2p model at the seafloor, carried out in this piece of work, gives the opportunity to assess possible extreme values.

In all 3 types of models the CO_2 is injected into the Tubåen Formation, located in zone 9, at two different point sources, either a virtual one or a realistic one. In the faulted and the generic chimney scenarios, the real injection point has been chosen, corresponding to the real location of the CO_2 injection well, located at about 2600 m below the upper grid boundary (Figures 2, 3a and 3b), with coordinates as shown below. For the realistic gas chimney scenarios (Figures 2 and 3b), the virtual injection well has been placed close to the gas chimney edge (Table 7). In order to increase the speed of simulation runs we aimed at constructing grids, for the realistic gas chimney scenarios, with a minimum amount of grid cells. In this attempt we were obliged to adopt a virtual injection well location as using the real injection well location would have created unmanageable grids (Figure 2).

Table 7. Coordinates of the real and virtual injection point

Injection point (given in the standard Transverse Mercator coordinate system (UTM) with an Easting, x-coordinate, and a Northing, y-coordinate, in meters)	
Real	**Virtual**
502130 m $< x <$502170 m	504380 m $<$ x $<$504420 m
7945890 m $<y<$ 7945910 m	7948880 m $<$ y $<$7948920 m
z $>$2570 m	2720 m $<$ z $<$ 2820 m

The overall injection rate is set at 0.7 Mt/year and is applied for 20 consecutive years, followed by 1980 years of simulation time without injection. Initially the whole simulation domain is saturated with brine and the pressure is hydrostatic. Except for the lower boundary, on which a Neumann no-flow condition is applied, all boundaries are defined as hydrostatic Dirichlet boundaries. The temperature, which is of interest when it comes to calculating the current phase states, is determined to be 4 °C at the sea floor and to rise linearly, at about 0.03 °C per meter, with increasing depth.

During this 2000-year period the total CO_2 migration, measured in [kg/s], from the storage site, the interlink flux, in [kg/(s m2)], and the current amount of CO_2, in [t], stored within the aquifer, were recorded.

The reservoir in the gas chimney scenarios was closed off and boundary conditions were applied in order to avoid "leakage" at the boundaries. In the faulted scenarios the Jurassic faults prevent CO_2 from escaping out of the model

domain and into the reservoir level and thus the boundary conditions were left open.

In future research it would be necessary to address the effect of the variation of boundary conditions on potential CO_2 leakage. The variation of boundary conditions strongly affects the CO_2-plume distribution. It's also important to determine appropriate boundary conditions not only for the reservoir but also for the other formations as different choices of boundary conditions strongly affect the time variation of the pressure field and the CO_2 plume distribution. In such an approach, boundary conditions for the fluid flow simulations can be based on knowledge of pressure support or known in/out-fluxes to/from a formation (Eigestad et al. 2009).

Simulation results

Before presenting the simulation results we will explain what each figure in this section intends to show. For a more detailed explanation of what each subfigure shows please consult the figure captions section at the end. Figure 4 presents results related to various fault scenarios. This includes graphs of fault permeability and fault thickness against ΔT1, for various average permeabilities. Figure 4 also plots the variation of caprock fault model scenarios (F1-F19) against ΔT2/ΔT1. Finally we can visualize how fault thickness and fault permeability variation affect the percentage of CO_2 "leaked" at reservoir level at the depth of 2300 m.

In figure 5 we present the results of the simulations on the realistic gas chimney scenarios. We present the effect of the variation of various parameters, such as gas chimney permeability or zone 9 permeability, on the percentage of CO_2 "leaked" at various recording levels, such as at 370 m, 600 m and 2300 m depths. We also aim to illustrate how the realistic chimney permeability variation and the permeability of zone 9 variation affect the maximum flux at various depths, such as at 2300 m (reservoir level) and 370 m depth.

Finally, in figure 6, we present the results of the generic gas chimney scenarios. Here, we illustrate how the generic gas chimney width variation affects the total percentage of CO_2 leaked at depths of 370 m and 2300 m and for scenarios containing either 1 or 2 generic gas chimneys. We also show how the average permeability variation affects ΔT1 at various depths, such as at 2300 m and 370 m depths.

When interpreting the simulation results it's important to take into account the various physical mechanisms involved in fluid flow and the leakage process. Upward migration of CO_2 is driven by pressure induced advection and buoyancy. Advection corresponds to a transport mechanism of a substance or conserved property by a fluid due to the fluid's bulk motion, whereas buoyancy can be defined as the tendency of a body to float or rise when submerged in a fluid.

The permeability characteristics of the rock layers overlying or adjacent to the geologic sinks thus becomes important. The permeability of the rock is a measure of the ease of convecting fluids through it and as such the permeability of the rock layers overlying or adjacent to the geologic sinks will affect how fast and how far the CO_2 will migrate. The hydrologic properties of the formations containing the geologic sinks should also be considered as they affect the potential for CO_2 leakage.

Permeability is a more important parameter affecting the CO_2 migration process. Uncertainty in porosity has less influence on CO_2 mass migration than the uncertainty in formation permeability (Gonzalez-Nicolas et al. 2012). Therefore, we focus on the variation of permeability. the

For the realistic and generic chimney scenarios the data is measured at three locations (Table 8). For the faulted scenarios the flux is measured only at 2300 m depth as the zones above are not modeled.

Table 8 (Flux measurement locations for chimney scenarios)

		Measurement Locations
		z location [m]
Flux	1	*370*
	2	*600*
	3	*2300*

For discussing the results, the following model outputs were considered: the percentage of "leaked" CO_2 after 50 years from the start of injection, the maximum flux within the 2000 year simulation period, the time when CO_2 migration starts (ΔT1) (Figure 4a), the time between the start of migration and when 3% of the total injected CO_2 has been "leaked" (ΔT2), and the ratio of the two times (ΔT2/ΔT1).

The reader should be made aware that this study is based on hypothetical leakage scenarios which may force faults or gas chimneys to leak CO_2 explaining our reference to the mass of CO_2 leaked. The language referring to leakage of CO_2 is part of the modelled scenarios and connected to the results from the adopted geological models. The simulation results do not imply or indicate that CO_2 has actually leaked or will leak from the Snøhvit reservoir.

Faulted caprock scenarios

In general, there is an increase of the percentage of CO_2 "leaked" mass and the maximum flux at 2300 m (reservoir level) with an increase in average permeability and with an increase in fault thickness (Figure 4e). The increase in fault thickness has a bigger effect on the percentage of CO_2 "leaked" as average permeability decreases (see decrease in steepness of slopes of the average permeability curves as average permeability increases in Figure 4e). This same trend is also valid in the plots of max flux at 2300 m depth vs fault thickness. Thicker faults have bigger impacts on CO_2 leakage because the thicker the fault, the larger the rock volume in the fault zone and the higher the pore space through which CO_2 can penetrate and potentially flow through.

For the fault permeability there is a different trend depending on the average permeability. For low average permeability, the percentage of CO_2 "leaked" mass after 50 years increases with increasing fault permeability but for medium and high average permeability they both decrease with increasing fault permeability (Figure 4d).

In general, with increasing average permeability, increasing fault thickness, and increasing fault permeability, there is a decrease in all the observed times (the time when

CO_2 migration starts, $\Delta T1$, and the time between $\Delta T1$ and when 3% has "leaked" i.e. $\Delta T2$); thus, the migration of CO_2 starts earlier (Figures 4a and 4b). At low fault permeability the curves are far apart and as fault permeability increases all curves come closer to each other. Slopes corresponding to low average permeability scenarios are steeper than the slopes for high average permeability (Figures 4a and 4e). The decrease is thus faster (see variation in slopes) for the lower average permeability scenarios.

As fault thickness increases, the average ratio $\Delta T2/\Delta T1$ increases (Table 9). There is no obvious trend for low average permeability scenarios and the effect of fault permeability on it is variable. $\Delta T2/\Delta T1$ decreases when moving from 50 to 100 mD fault permeability and then increases from 100 to 300 mD (Figure 4c). The decrease is sharper than the increase (see high average permeability scenarios part of Figure 4c and Tables 4 and 9).

Table 9. Important ratios for the faults scenarios

Scenario	Fault Thickness	$\Delta T2/\Delta T1$	Average $\Delta T2/\Delta T1$
F1	50	0.66	
F3		0.59	
F4		0.60	
F5	150	0.74	
F6		0.63	
F7		0.67	
F8	50	0.51	0.60
F9		0.48	
F10		0.43	
F11	150	0.40	0.68
F12		0.50	
F13		0.72	
F14	50	0.82	
F15		0.64	
F16		0.67	
F17	150	0.87	
F18		0.77	
F19		0.85	

In the high average permeability scenarios, we encounter the lowest $\Delta T2/\Delta T1$ numbers for the 100 mD fault permeability. This is clearly observed by looking at the bottom of the "wave" in scenarios F15 and F18, which have the lowest $\Delta T2/\Delta T1$ numbers, which correspond to scenarios with a 100 mD fault permeability. Having the lowest $\Delta T2/\Delta T1$ numbers signifies that the ratio of CO_2 migration duration vs the period until start of migration is the smallest.

The smallest $\Delta T2/\Delta T1$ ratios are observed for the low average permeability scenarios (Figure 4c). There is a longer period before CO_2 migration and then a relatively faster period of CO_2 migration.

Realistic gas chimney scenarios

An increase in average permeability results in a clear increase of the ratio of CO_2 "leaked" and the maximum flux measured at all depths; 370 m and 2300 m (Figure 5).

Chimney permeability has a similar influence on the CO_2 "leaked" and the maximum flux as the average permeability (Figures 5a, 5b and 5f). An increase in chimney permeability results in a small increase of both parameters. At 370 m depth there is a stronger increase of the percentage of CO_2 "leaked" when going from 343 to 765 mD (Figure 5a). At 370 m depth, we are measuring potential CO_2 leakage at near seabed level, far away from the reservoir. CO_2 needs more time to reach this depth, thus explaining the smaller percentages of "CO_2 leaked" at this depth for all different average permeabilities. It also has to go through the less permeable layers that are located above the gas chimneys, which play an important role in controlling the upward flow of CO_2.

For the step from 765 to 3000 mD the increase is smaller; the change in slope is especially visible in the high average permeability case scenario (see change in slope of all curves as chimney permeability increases in Figure 5a). At 600 m depth the increase between 343 and 765 mD and 765 and 3000 mD is more or less equivalent. At 2300 m depth there is nearly no difference in the fraction of CO_2 "leaked" when varying chimney permeability, i.e. along the curves for all the 3 curves (Figure 5b). So at this level only, chimney permeability has no influence at all as all 3 curves are nearly horizontal (Figure 5b).

The permeability of zone 9 has the lowest influence but the variation range is smaller (Figures 5c and 5d). For medium average permeability the increasing permeability in zone 9 results in a decrease of CO_2 migration both at 600 m (Figure 5c) and 2300m (Figure 5d) depths. For low average permeability the increasing permeability in zone 9 results in an increase of CO_2 migration both at 600 m (Figure 5c) and 2300 m (Figure 5d) depths. Here permeability in zone 8 measures 20 mD.

An increase of the reservoir permeability results in an increase of the max flux for all scenarios with low average permeability at various depths (Figure 5f). For the medium average permeability however, the max flux decreases with increasing reservoir permeability (Figure 5f).

Generic gas chimney scenarios

In general, maximum fluxes and the percentage of CO_2 "leaked" after 50 years at 2300 m are larger than at 370 m depth because we are closer to the injection point (Figure 6).

At 2300 m depth an increasing chimney width clearly results in an increase of the percentage of CO_2 "leaked" after 50 years from the start of injection (Figure 6b). At 370 m, for smaller chimney widths, the percentage is slightly higher (see negative slope of curves in Figure 6b), and no real difference is observed between 400 m and 600 m chimney widths. At the end of the simulation period, at 370 m, the total percentage of CO_2 "leaked" is higher for the 600 m chimney width compared to the 200 m chimney width (Figure 6a). The difference in the curves at 370 m between 50 and 2000 years after start of injection illustrates that these abrupt changes in percentage of CO_2 "leaked" are time dependent.

At 370 m the determining parameter is now the average permeability and time and not the chimney width (Figure 6). The variable ranking within the permeability classes shows that whatever the chimney width maybe it doesn't affect the overall ranking for average permeability (Figure 6).

ΔT1 decreases with increasing average permeability (at least at the beginning) (Figure 6c). This ΔT1 decrease is more important at 370 m than at 2300 m depth (compare continuous and interrupted lines in Figure 6c). Therefore average permeability plays a more important role, in terms of the effects it has on ΔT1 time, at 370 m than at reservoir level.

The percentage of CO_2 that "leaks" after 50 years from the start of injection, whether at 370 m or 2300 m depth, is always higher when there are 2 chimneys than when there is only 1 chimney simulated (Figure 6d). At 2300 m depth, both for 1 and 2 chimneys there is an increase of the percentage of CO_2 "leaked" as the chimney width increases (Figure 6).

At 370 m depth, the above trend is not observed. For the 2 generic chimneys there is a clear kink at 200 and 400 m chimney widths, with an increasing percentage of CO_2 going from 400 m to 200 m and to 600 m chimney width, since at 200 m chimney width the CO_2 is more concentrated in that more confined volume so pushed up faster (Figure 6e). This trend is also followed for the 1 chimney scenarios but for later time periods (Figures 6a and 6b) (compare the 1 and 2 chimney curves for various average permeability scenarios in Figure 6e). So the number of chimneys affects the percentage of CO_2 "leaked" after 50 years at this specific depth. At 2300 m an increase in the percentage of CO_2 "leaked" with increasing chimney width is observed whatever the average permeability and whatever the number of chimneys maybe.

The number of chimneys becomes an important parameter only at a shallow depth, e.g. at 370 m depth. At shallower depths there is less overburden rock, gravitational forces are weaker and CO_2 gas is less constrained and can thus cover a larger volume and pore space. Under such circumstances increasing the number of gas chimneys, at shallow depths, adds a supplementary factor that favors the percentage of CO_2 leaked. The effects of chimney number variation and buoyancy could also be clearly illustrated by using the parameter of relative percentage change.

Discussion
Faulted caprock scenarios

The differences in petrophysical properties such as permeability, between fault zones and neighboring reservoirs, are believed to be the result of one or more physical processes associated with the deformation that occurs in fault zones (Bennett et al. 1998). The gravitational number (Gr), an important factor in the interpretation of the results, corresponds to the ratio of gravitational to viscous forces (Kissinger et al. 2014) and can be used to compare these physical processes:

$$Gr = \frac{(\rho_B - \rho_{CO2})g\,K}{\mu_{CO2}\,\frac{\dot{m}_{CO2}}{\rho_{CO2}}}$$

Where:

ρ_B = brine density [kg/m³],
ρ_{CO2} = CO_2 density [kg/m³],
g = acceleration due to gravity in [m/s²],
K = intrinsic permeability in [m²],
μ_{CO2} = dynamic viscosity of the CO_2 in [Pa s],
$\dot{m}_{CO2}$ = specific mass injection rate in [kg/s/m²].

For high Gr the gravitational forces predominate and the CO_2 will move quickly to the caprock and will distribute as a thin layer under the caprock indicating a poor storage efficiency of the reservoir. For low Gr the viscous forces are more dominant and the CO_2 will spread over the entire depth of the reservoir using a cylindrical propagation front. In this case there is a better usage of the given pore space and more residual trapping occurs. An increase of the average permeability increases the gravitational forces and Gr (Kissinger et al. 2014; Nordbotten and Celia 2012). More CO_2 will reach the fault as the CO_2 is preferentially pushed towards the caprock and the area where the fault cross cuts the caprock.

It's essential to note here that the storage capacity of the reservoir referred to above, corresponds to the modeled storage capacity of the reservoir. Its lateral extent is determined by the modeler according to the characteristics in Table 3 and vertically it corresponds to zones 8 and 9 of the models, see Annex Table 1. For low average permeability (small Gr) the CO_2 is spread over the whole depth and more CO_2 is stored in the reservoir (Figure 7a). Thus the percentage of CO_2 "leaked" and the maximum flux are smaller. In addition the CO_2 migration starts earlier for high Gr (high average permeability) because the CO_2 moves faster beneath the caprock and reaches the fault earlier.

There is a difficulty to start the migration process when the average permeability is low. CO_2 moves slower from the injection point to the faults. Injection into geologic formations will tend to diffuse the CO_2 as it moves away from the injection point. At low average permeability, the distance to the injection point and the average permeability become determining factors.

At this point of the discussion, in order to help the thinking process and draw conclusions, it helps to remind that regarding the modeling of the injection operations, the injection rate applied was set at 0.7 Mt/year and applied over a period of 20 consecutive years. In total 14 Mt of CO_2 have been injected from either a theoretical or a realistic well injection location. We thus considered, in a holistic way, the amounts of CO_2 injected, the locations from which it is injected, the distances the CO_2 could migrate and the time factor for the various processes involved.

An increase of the fault thickness increases the area which can trap CO_2 and reduces the distance between the fault and the injection point. Thus thicker faults result in higher percentage of CO_2 migration, higher maximum CO_2 migration rates and earlier migration.

For the variation of fault permeability a different behaviour for different average permeabilties is observed. For low average permeability, an increase in fault permeability results in an increase of the percentage of CO_2 migration and maximum flux. Here the difference between the permeability in the reservoir and the fault is very high. Thus for an increase of fault permeability the fault acts more and more as a preferential flow path. High fault permeability creates a strong gradient into the fault, which gives faster migration into it.

For MEDIUM (zone 8/9: 200/500 mD) and HIGH (550/880 mD) reservoir average permeability the difference between the average and fault permeability is small (fault permeability = 50-300 mD), thus it seems that the preferential flow path develops laterally in the reservoir instead of vertically through the fault. Apparently the pressure in the

reservoir is here of importance. We have made the assumption that the same amount of CO_2 is injected for each case, thus an increase in the fault permeability may lower the pressure in the reservoir and less CO_2 reaches the fault. The degree by which the reservoir pressure might fall will depend on the amount of injected CO_2.

Under the following conditions (low average permeability and low and high fault thickness), any increase in fault permeability will have a greater effect on fluid flow and on the time of start of CO_2 migration. Also when using the low average permeability scenarios, any increase in fault thickness will lead to a larger percentage of "leaked" CO_2 compared to when using higher average permeabilities.

As fault thickness increases, propensity to leak becomes higher. With thicker faults it becomes easier for CO_2 migration to occur, as it's illustrated by the average values per fault thickness calculated in Table 9. For a 50m fault thickness, $\Delta T2/\Delta T1=0.6$ and for a 150m fault thickness it's 0.68. A higher $\Delta T2/\Delta T1$ ratio signifies a lower $\Delta T1$ compared to $\Delta T2$. This means a relatively shorter period until the start of CO_2 migration for thicker faults.

For high average permeabilities, 100 mD is the optimum fault permeability, allowing for CO_2 migration to occur at the fastest possible pace (Figure 4c). For low average permeability the variation in fault permeability and thickness has greater effect than for medium and high average permeability (Figures 4a and 4e). In low average permeability conditions the fault permeability is larger than the reservoir permeability and thus the fault will act as a preferential pathway for CO_2 migration.

Realistic gas chimney scenarios

The gas chimney structure is characterized by high intrinsic permeability leading to a high mobility of the CO_2 phase. As a result, the overpressures needed for the creation of a migration pathway able to transport 22.2 kg/s are much smaller than in the simulations run without these geological features.

The average permeability strongly influences the CO_2 migration at all depths (Figure 5a-5d). For higher average permeability the CO_2 can distribute faster in the reservoir (zone 8 belongs to the reservoir) and during the entire 2000-year period more CO_2 reaches the chimney. There is still CO_2 migration taking place after 2000 years. As in the fault scenarios, this can be validated by Gr.

The following effects can explain the behaviour of the percentage of CO_2 "leaked" and the maximum flux for varying chimney permeability (Figure 7b). At near surface depths the permeability of 765 mD is already large enough for a significant CO_2 flow; therefore there is no influence of a further increase. Even if we assume that leakage may occur through these structures, observations at natural seeps and release experiments revealed however, that the footprint at the seabed where organisms would be impacted by CO_2 is small for realistic leakage scenarios (ECO2 2014; ECO2 2015).

But at the chimney top level (600 m), a further increase from 765 to 3000 mD has an additional effect on improving CO_2 flow. This is probably because this measurement is taken right at the top of the chimney and therefore this reflects the chimney effect without the influence of the background rocks between the chimney top (600 m) and at 370 m depth.

The chimney permeability influences the total CO_2 escaped at the top (Figure 5a). For the 342 mD chimney permeability, compared to the 3000 mD one, for example (Figure 7b), the plume shape is smaller but more CO_2 reaches the chimney at a second location. The increase in percentage of CO_2 migrated is observed more clearly for the change from 343 to 765 mD (see steeper slopes in Figure 5a) compared to the change from 765 to 3000 mD (see how slopes become less steep, Figure 5a). An increase in CO_2 migration rate can be explained by the increase of the CO_2's mobility. Additionally, the pressure gradients at the phase boundaries force the CO_2 phase into fully brine-saturated areas and thus the fluid flow pathways are becoming wider.

For medium average permeability the increasing permeability in zone 9 results in a decrease of CO_2 migration (Figures 5c and 5d). For medium average permeability the permeability in zone 8 (reservoir) is 200 mD. The CO_2 will rise into zone 8, distribute in this zone due to the high permeability there and thus the influence of zone 9 will be small.

For low average permeability, the increasing permeability in zone 9 results in an increase of CO_2 migration both at 600 m (Figure 5c) and at 2300 m (Figure 5d) depths. Here permeability in zone 8 is only 20 mD. The CO_2 spreading in zone 9 is more developed. For smaller permeabilities in zone 9 the pressure in the reservoir is increased. Thus the CO_2 is spread over a larger domain and the chimney is reached over a larger region.

As the permeability of zone 9 increases, the difference in permeability between the zones 9 and 8 increases, as does also the potential and the ease of flow from zone 9 towards zone 8, which explains also the increase in percentage of CO_2 "leaked".

At all depths, average permeability becomes a less important factor in the CO_2 migration process when permeability of zone 9 increases. This can be observed by how the low average permeability and the medium average permeability curves are far apart at low permeability of zone 9 values and as permeability of zone 9 increases this gap decreases (Figures 5c and 5d). Therefore at low permeability of zone 9, average permeability is a determining factor.

There is a strong interaction between average permeability and zone 9 permeability. Depending on the ratio the trend for increasing permeability of zone 9 changes. The same trend is observable at all depths (Figure 5c). Depending on the average permeability and the permeability in zone 9 the CO_2 is spread differently over the total domain (Figures 5a and 5c). Thus the chimney is reached at different locations. If a larger chimney area is reached, the storage capacity in the chimney increases and less CO_2 migration occurs at the top.

At all depths, at low permeability of zone 9, average permeability becomes a determining factor in the CO_2 migration process (Figures 5c -5d).

Generic gas chimney scenarios

The same influence of the average permeability, as in the two different kinds of scenarios presented before, is observed. The percentage of CO_2 that escapes and the maximum flux

strongly depends on the following parameters and their interaction: average permeability, the diameter of the chimney, the distance to the injection site, the depth at which we are measuring and the residual saturation (Figure 6).

The average permeability influences the plume shape within the reservoir and for larger average permeability more CO_2 leaks (Figure 7c). An increased chimney width results in a larger amount of CO_2 that migrates at 2300 m because of the larger capturing area and the smaller distance to the injection point (Figure 6). At 2300 m the influence of the chimney width on the amount of CO_2 that has migrated is stronger (see steeper slopes in Figure 6) than at 370 m, (see decrease in steepness of slopes, Figure 6).

For the CO_2 migration at 370 m, the percentage of CO_2 migration for the chimney width of 600 m is the highest, followed by 200 m and 400 m (Figure 6a). This trend is a time dependent process and begins first at later time steps, (compare Figure 6b after 50 years and Figure 6a after 2000 years). After 50 years this kink is only slightly visible. It is an interaction of the diameter of the chimney, the distance from injection and the storage capacity within the chimney which is dominated by residual saturation.

In general, larger storage capacity of gas chimneys does not mean larger chimney permeability. However, we have noticed at 2300 m depth that an increased chimney width results in a larger amount of CO_2 that migrates, probably because of the larger capturing area and the smaller distance to the injection site (Figure 6). In a larger chimney the storage capacity is potentially higher because more CO_2 can be residually trapped within the larger volume.

For the 600 m chimney the residually trapped mass is probably higher than in the 400 m and 200 m chimneys. However, the amount that migrates into the chimney is still very large and dominates the situation. Thus, the amount of CO_2 that migrates at 370 m is still the largest for the 600 m chimney. For the 400 m chimney there is less CO_2 entering the chimney at 2300 m depth and thus in total less CO_2 than in the 600 m chimney scenario reaches the top (370 m). However, the total amount is also smaller compared to the 200 m case. In the 400 m case more CO_2 can be trapped residually than in the 200 m case. Here dominates the residual trapping instead of the influence of the larger diameter of the chimney and the distance to the injection site.

The number of chimneys becomes an important parameter at reservoir depths e.g. 2300 m (Figure 6d), where the number of chimneys affects more the percentage of CO_2 "leaked" than at 370 m (Figure 6e). With more chimneys the volume covered by the chimneys is increased and thus more CO_2 can migrate.

In Figure 7c one chimney of a width of 200 m exists in a low average permeability field. We also observe the case with two chimneys of 600 m width within a high permeability field (Figure 7c). Although we cannot clearly see the effect of the chimney number variation on the amount of CO_2 leaked, we notice that, in this second case with the two gas chimneys, the CO_2 plume rises faster underneath the caprock and a larger amount of CO_2 reaches the two larger chimneys than in the first case. In future simulations we could set certain parameters the same in order to visualize the effect of the chimney number variation on CO_2 leakage.

The time of start of migration depends on the distance from injection and the relative permeability. The time when CO_2 migration at the top, at 370 m depth starts, is strongly influenced by the amount of CO_2 that escapes out of the reservoir and the saturation in the chimney (Figure 6c), which is influenced by the chimney diameter. A higher saturation results in higher relative permeabilities thus the CO_2 moves faster and arrives earlier at 370 m depth (Figure 6c).

The CO_2 leaks earlier for higher average permeability. The fastest CO_2 migration occurs for the 600 m chimney width (Figure 6c). In this case the largest amount of CO_2 leaks out of the reservoir and although a lot of CO_2 can be trapped residually due to the large chimney the saturation is large enough for a high relative permeability. Thus, the movement will be fast. For the 400 m chimney width, CO_2 migration occurs at the latest possible time. Here, less CO_2 than in the 600 m case leaks out of the reservoir and a lot of CO_2 is trapped residually thus the relative permeability is low and CO_2 moves slower. In the 200 m case, even less CO_2 migrates out of the reservoir (Figure 6c).

Conclusions

Leakage of CO_2 is observed in the modelled scenarios, but only as a result of the modelling and simulation work carried out in this study. There is currently no leakage of CO_2 taking place from the Snøhvit reservoir.

In the modelled scenarios, the variability of CO_2 mass "leaked" in (%) in proximity of real gas chimneys, faults and generic gas chimneys/abandoned wells was analyzed. The analysis took into account the uncertainty associated with the permeability of reservoir rocks and rocks in the rest of the modeled domain (Table 1 annex) and uncertainty on the permeability and other parameters related to fluid flow pathways such as gas chimneys (Table 1) and faults.

Among the investigated uncertain parameters, the one that had the most influence on the CO_2 migration process was probably the permeability of the reservoirs and especially the average permeability. CO_2 migration was also very sensitive to the uncertainty from the permeability of fluid flow pathways and to the type of statistical distribution used to characterize it (Gonzalez-Nicolas et al. 2012). Depending on the gravitational number the plume shape changes and the leakage rates are strongly affected.

In the caprock fault models, fault thickness and the contrast between average permeability and fault permeability are important parameters at Snøhvit. When the average permeability is low, there is a difficulty to start the CO_2 migration process, and the variation in fault permeability and thickness has greater effect than for medium and high average permeabilities. Under low average permeability conditions any increase in fault thickness will have a bigger effect on the fraction of CO_2 migrated. Also, for the faulted caprock scenarios, we came to the important conclusion that at near surface depths the permeability of 765 mD is already large enough for a significant CO_2 flow; therefore there is no influence of a further increase. But at the chimney top level (600 m) a further increase from 765 to 3000 mD has an additional effect on improving CO_2 flow. More simulations can be carried out, using other fault thicknesses and permeabilities of around 100 mD, to determine exactly what the optimum fault permeability is that allows for the lowest $\Delta T2/\Delta T1$ ratio.

In the realistic chimney scenarios the average permeability parameter has a major influence on the CO_2 migration process. It strongly influences the CO_2 migration at 370 m depth. At all depths and at low permeability of zone 9, average permeability becomes a determining factor in the CO_2 migration process. In this scenario group, chimney permeability is a less influential factor. Chimney permeability influences the total CO_2 migrated only at the top of the chimney. At reservoir level, chimney permeability has nearly no influence at all on the fraction of CO_2 migrated.

Finally, in the generic gas chimney scenarios also the average permeability strongly influences the maximum flux and the total amount of CO_2 migrated. The total amount of CO_2 that migrates strongly depends on the interaction between average permeability, which strongly influences the plume shape and the velocity for the CO_2 movement, the diameter of the chimney, which influences the capturing area, and the storage capacity due to the residual saturation in the chimney, which is increased with increasing diameter. More simulations could be run with a greater number of chimneys, e.g. 3, 10, and introduce new parameters such as variation of location, form and vertical extent of chimneys to see what effect they can have on fluid flow.

In all modelled scenarios the caprock is characterized by a 10 nD permeability explaining why the upward migration into the caprock is a slow process. Upward migration of CO_2 is driven by pressure induced advection and buoyancy. Considering the slow upward migration velocity of the plume this geological setup can be regarded as a safe and suitable storage site. This can also be validated by the absence of any CO_2 observed at the seabed level or the seawater in the area.

If the injected CO_2, however, is lighter than the formation brine, this implies an upward-directed buoyancy force which may be sufficient for breaching the seal (Edlmann et al. 2013), when the CO_2 column exceeds a certain height.

Future leakage assessment activities have to focus on quantifying the hydraulic properties of seal by-passing fluid conduits by studying field analogues, using multi-frequency acoustic surveys and ideally drilling into these gas chimney structures at Snøhvit and elsewhere. Only a detailed knowledge about the hydraulic properties may help to quantify their actual leakage potential and thus potentially minimize the probability of CO_2 leakage in the modelled scenarios. Such knowledge, as well as better reservoir characterization, can also be integrated in monitoring strategies to mitigate the risk of CO_2 leakage (Edlmann et al. 2013; Schutze et al. 2012).
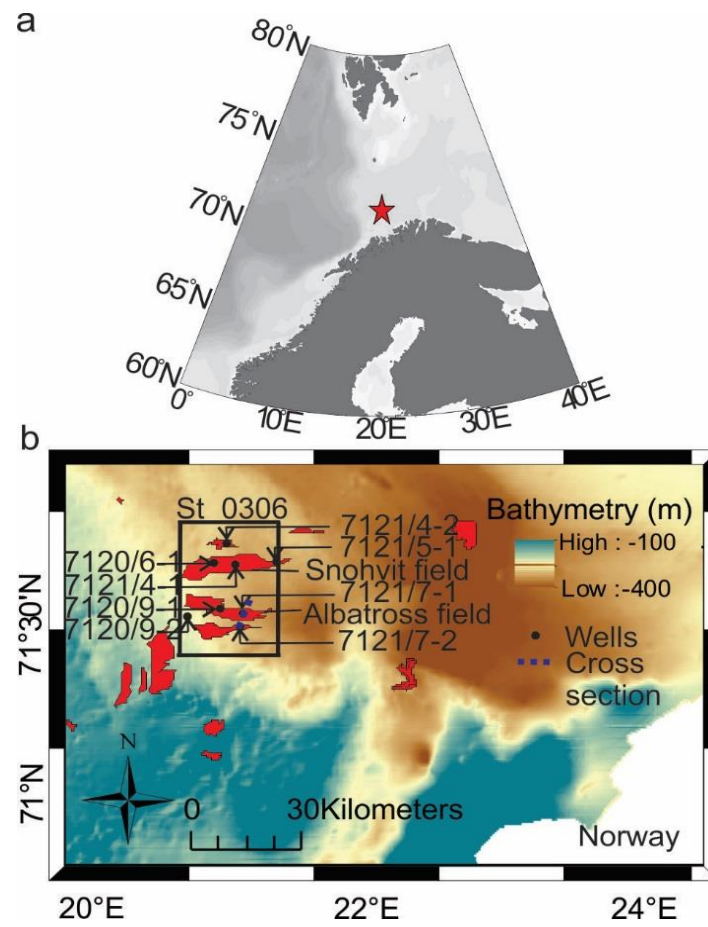
Figures

Fig. 1 Location of the study area (**a**) and overview of the study area (**b**) showing 3D cube ST0306.
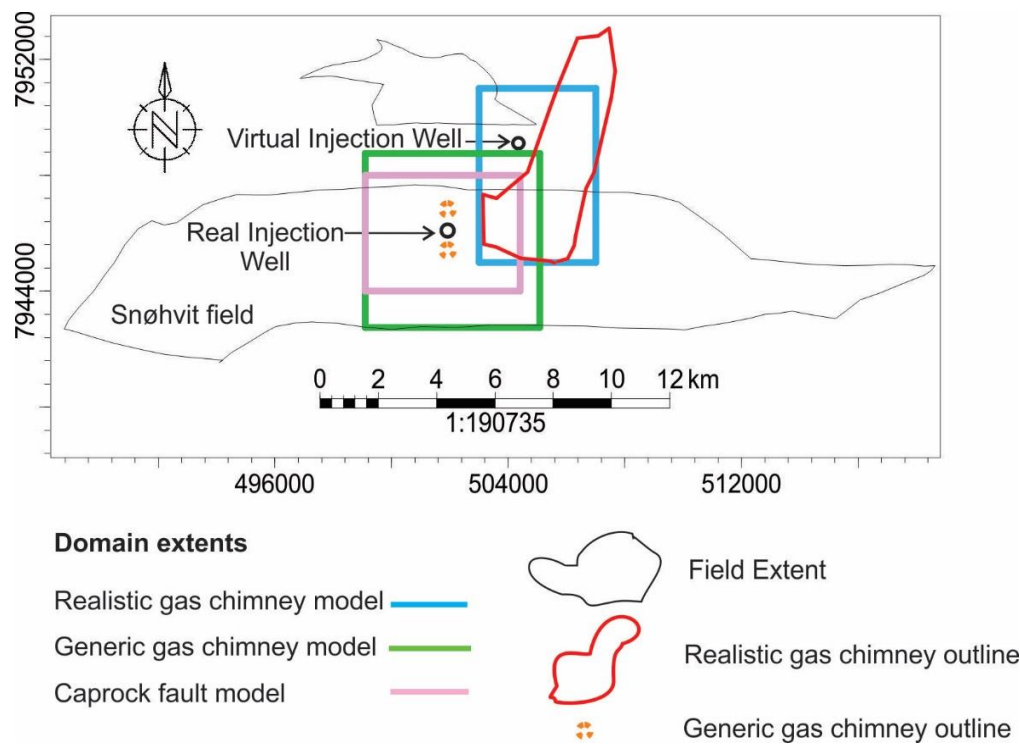

Fig. 2 Domain extents for the 3 types of modeling groups, namely realistic and generic gas chimney models, caprock fault models and location of modeled gas chimneys.
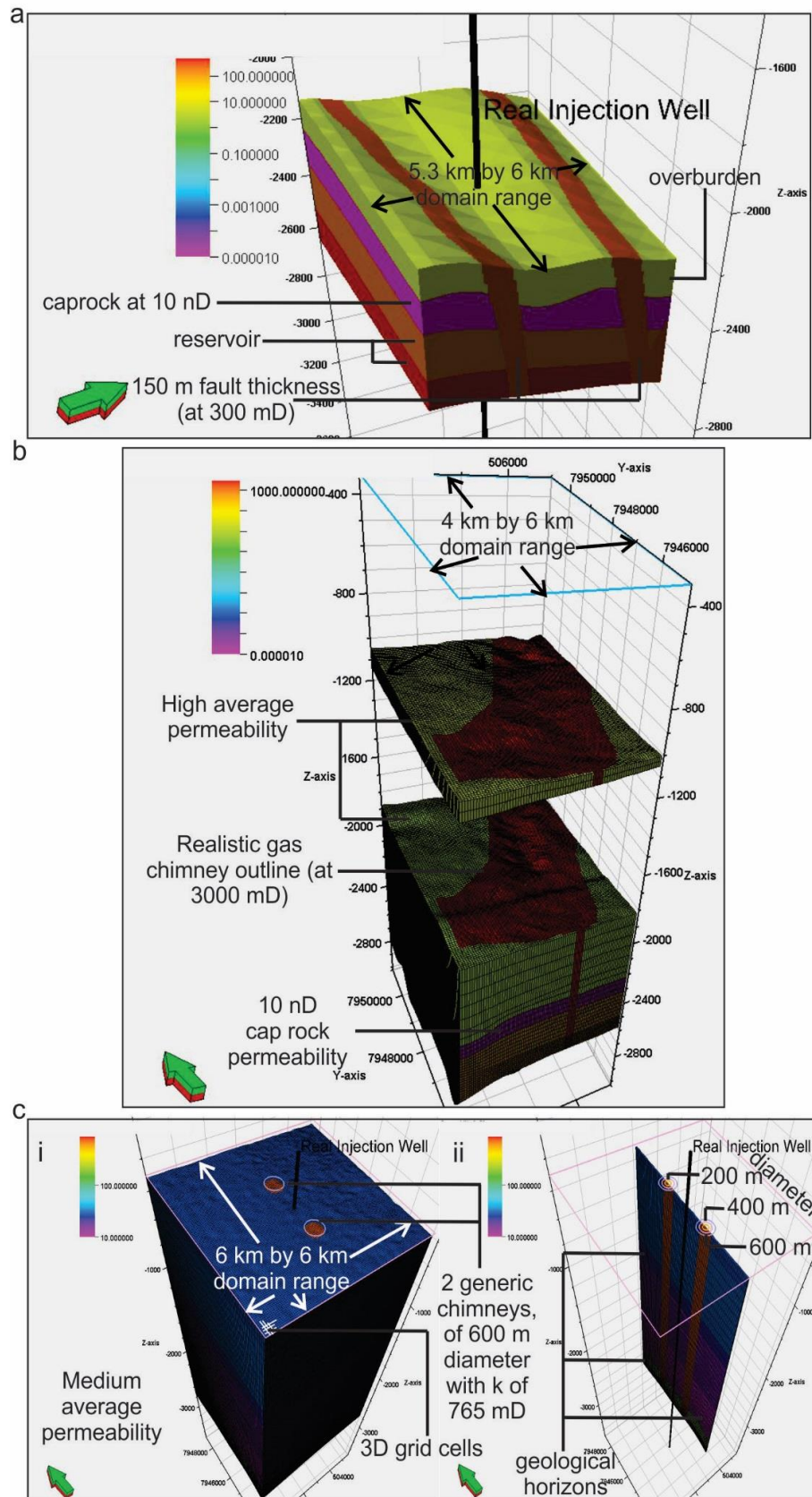
Fig. 3 Fault scenarios: Permeability model for the faulted caprock scenario F7 (**a**) (Medium average permeability, 150 m fault thickness at 300 mD), Realistic chimney scenarios: Permeability model for the realistic gas chimney scenario C17 (**b**) (High average permeability, 3000 mD in the gas chimney and 500 mD in zone 9) and Generic chimney scenarios: Permeability model for the generic gas chimney scenario G3 (**ci**) (Medium average permeability, 2 generic gas chimney of 600 m diameter and at 765 mD and (**cii**): cross section through the 2 generic gas chimneys.
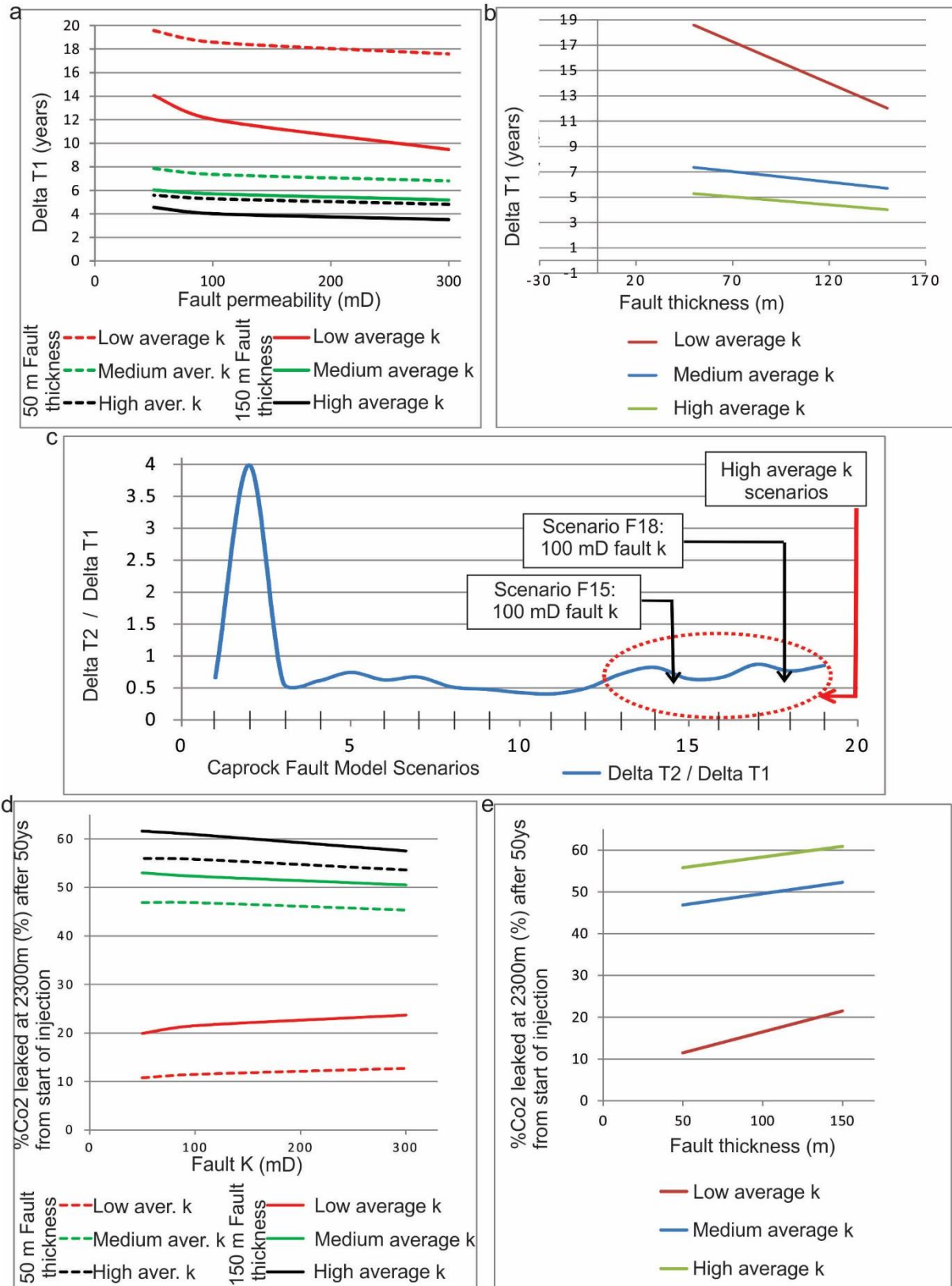
14

Fig. 4 Fault scenarios: Graph of fault permeability against ΔT1 (**a**) (the time from the beginning of the simulation until the start of CO_2 migration) for different average permeabilities and fault thicknesses, Graph of fault thickness (m) against ΔT1 (**b**), the time until start of CO_2 migration, for various average permeabilities, Graph of caprock fault model scenarios (F1-F19) against ΔT2/ΔT1 (**c**), Graph of fault permeability (mD) against the percentage of CO_2 "leaked" at 2300 m after 50 years from start of injection, for various average permeabilities and fault thicknesses (**d**) and Graph of fault thickness (m) against the percentage of CO_2 "leaked" at 2300 m after 50 years from the start of injection, for various average permeabilities (**e**).
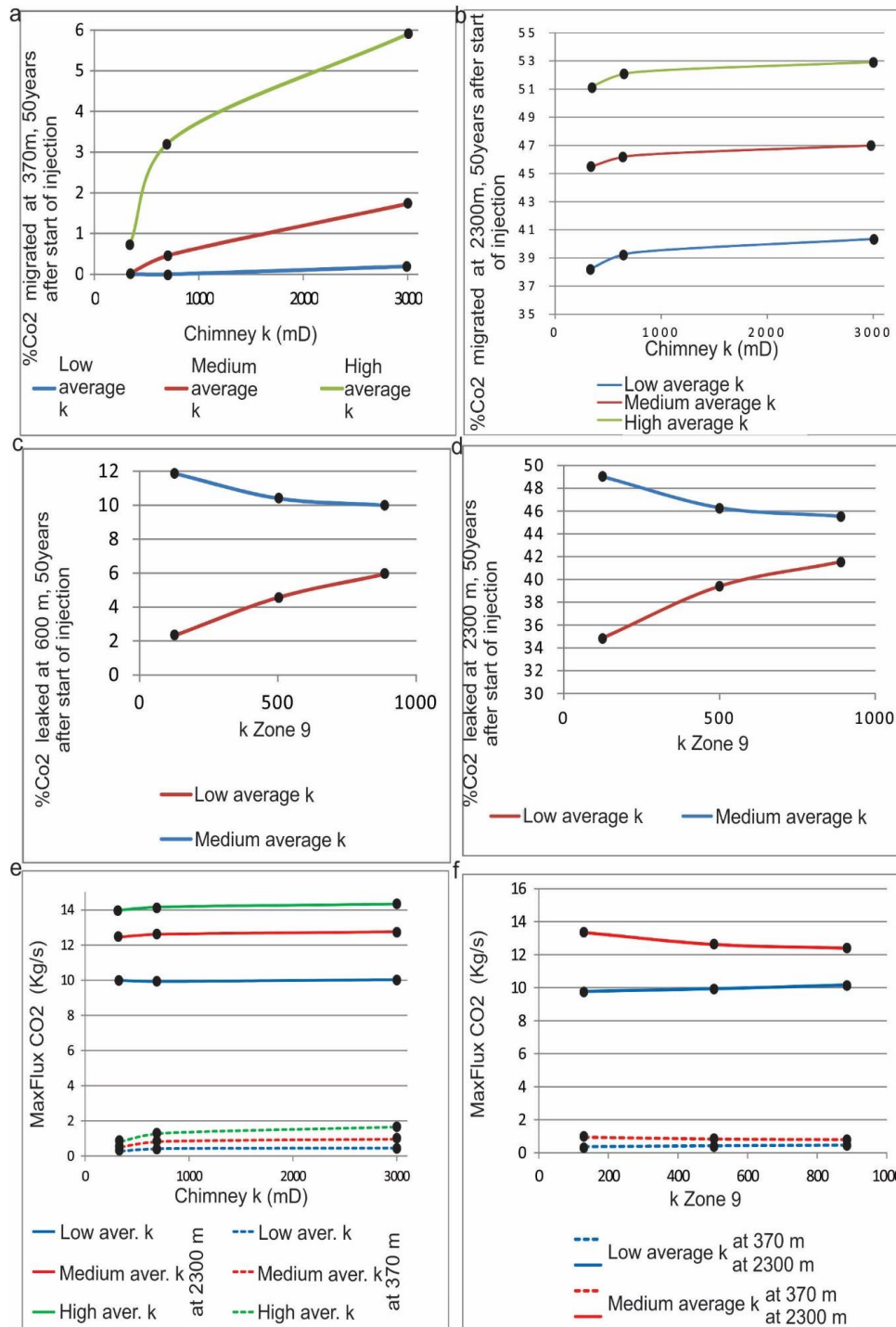
Fig. 5 Realistic chimney scenarios: Graph of chimney permeability against the percentage of CO_2 "leaked" at 370 m depth after 50 years from start of injection for various average permeabilities and at a constant permeability in zone 9 of 500 mD for the realistic gas chimney scenarios (**a**), Graph of chimney permeability against the percentage of CO_2 "leaked" at 2300 m depth (reservoir level) after 50 years from start of injection for various average permeabilities and at a constant permeability in zone 9 of 500 mD for the realistic gas chimney scenarios (**b**), Graph of zone 9 permeability variation against the percentage of CO_2 "leaked" at 600 m depth, after 50 years from start of injection for various average permeabilities and at a constant chimney permeability of 765 mD for the realistic gas chimney scenarios (**c**), Graph of zone 9 permeability variation against the percentage of CO_2 "leaked" at 2300 m depth (reservoir level) after 50 years from start of injection for various average permeabilities and at a constant chimney permeability of 765 mD for the realistic gas chimney scenarios (**d**), Graph of realistic chimney permeability variation against maximum flux at 2300 m depth (reservoir level) and 370 m depth after 50 years from start of injection for various average permeabilities and at a constant permeability of zone 9 permeability of 500 mD for the realistic gas chimney scenarios (**e**) and Graph of permeability of zone 9 variation against maximum flux at 2300 m depth (reservoir level) and 370 m depth after 50 years from start of injection for various average permeabilities and at a constant chimney permeability of 765 mD for the realistic gas chimney scenarios (**f**).
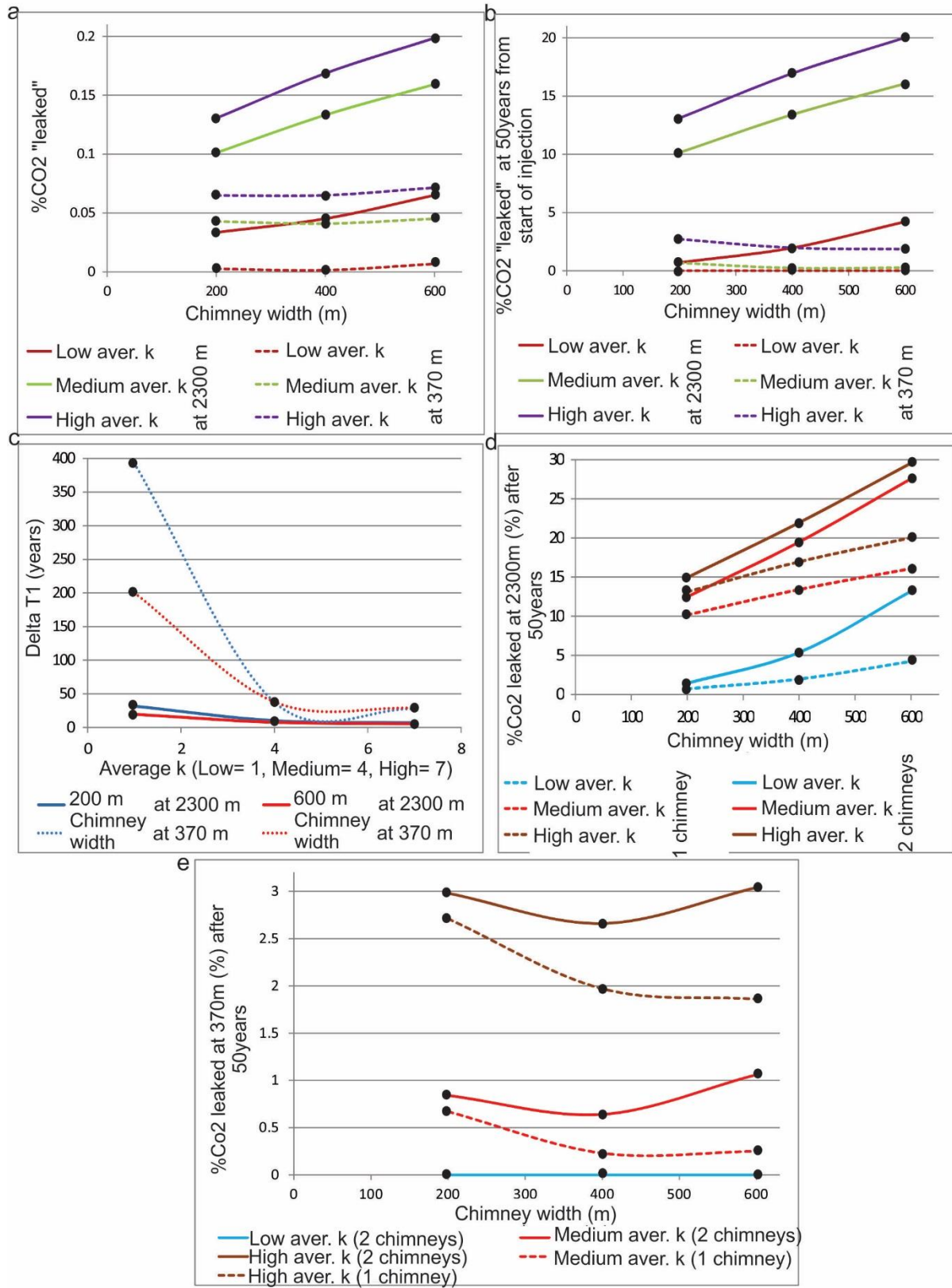
Fig. 6 Generic chimney scenarios: Graph of chimney width variation (m) against the total percentage of CO_2 leaked (**a**) and the percentage of CO_2 "leaked" at 50 years from start of injection at depths of 370 m and 2300 m and at constant chimney permeability of 765 mD and for scenarios with 1 generic gas chimney (**b**). Graph of average permeability variation against $\Delta T1$ at various depths, 2300 m and 370 m depth, and for a varying chimney width and for scenarios with 1 generic gas chimney (**c**), Graph of chimney width against the percentage of CO_2 "leaked" after 50 years from start of injection at depth of 2300 m and for various average permeabilities with either 1 or 2 generic gas chimneys (**d**) and Graph of chimney width against the percentage of CO_2 "leaked" after 50 years from start of injection at depth of 370 m and for various average permeabilities with either 1 or 2 generic gas chimneys (**e**).
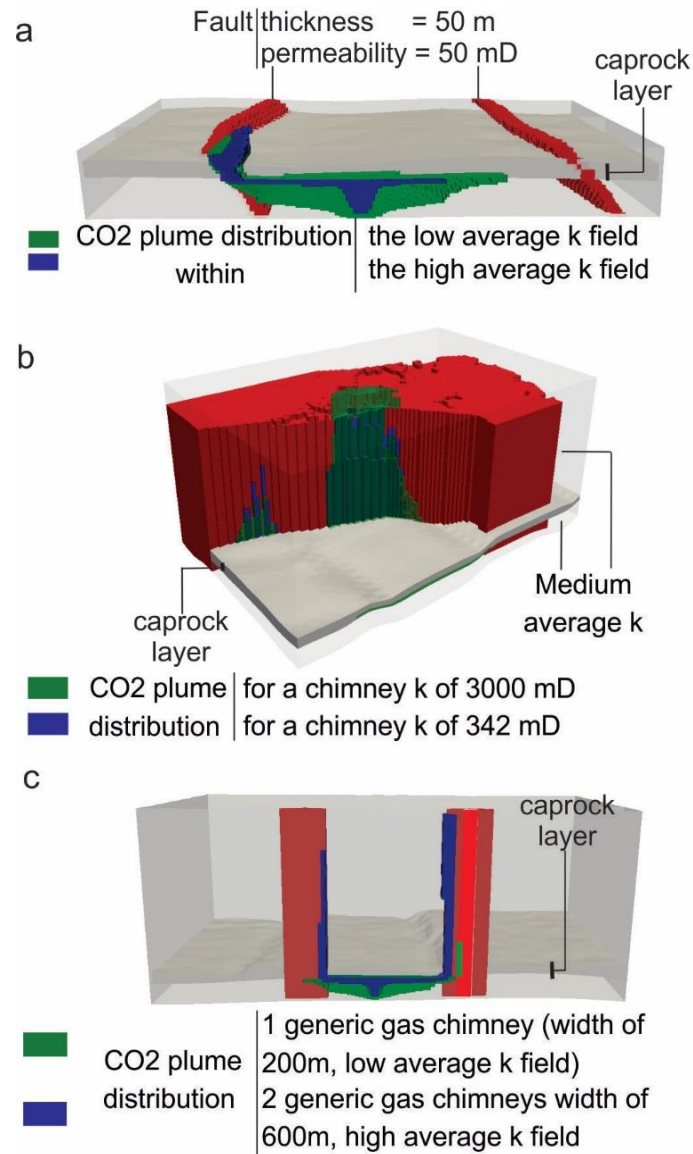
Fig. 7 Fault scenarios: CO_2 plume distribution after 50 years within the high (Scenario F14) and within the low (Scenario F8) average permeability field (Fault thickness: 50 m, fault permeability 50 mD. The red zone here corresponds to the fault zone, characterised by a fault permeability of 50 mD, which is not affected by any CO_2 migration) (**a**), Realistic chimney scenarios: CO_2 plume distribution after 2000 years for a chimney permeability of 342 mD (Scenario C2) and 3000 mD (Scenario C3) (medium average permeability, permeability of zone 9: 500 mD. The red zone here corresponds to the part of the realistic gas chimney in which no CO_2 plume distribution is observed) (**b**) and Generic chimney scenarios: CO_2 plume distribution after 50 years for a scenario with 1 generic gas chimney of a width of 200 m existing in a low average permeability field (Scenario G4) and for a scenario with 2 generic gas chimneys of a width of 600 m existing in a high average permeability field (Scenario G9) (**c**). The red zone here also corresponds to the parts of the generic gas chimneys in which there is no CO_2 observed)

Annex

Table 1: Petrophysical property variation for the subsurface at Snøhvit (Buenz et al. 2012)

Zones	Source	Average φ (%)	Average permeability (mD)	Av. φ (%)	Av. permeability (mD)	Av. φ (%)	Av. permeability (mD)
		SCENARIO					
		LOW		MEDIUM		HIGH	
1 (Nordland Gp)	PhiS 4 wells	18	21	23	28	28	34
2 (Torsk Formation)		33	23	36	31	38	39
3 (Kveite Formation)		30	16	33	22	35	28
4 (Kolmule Formation)		28	11	30	15	32	19
5 (Kolje Formation)		24	6	25	8	27	10
6 (Knurr Formation)		21	4	24	7	27	10
7 (Hekkingen Formation)	HRS 4wells	5	4	13	8	20	12
8 (Fuglen,Stø,Nordmela)	Literature	10	20	16	200	18	500
9 (Tubåen Formation)		10	130	15	500	20	880

In more recent models the caprock permeability has been changed to 10 nD (in zone 7)

References

Arntsen B, Wensaas L, Loseth H, Hermanrud C (2007) Seismic modeling of gas chimneys Geophysics 72:Sm251-Sm259 doi:Doi 10.1190/1.2749570

Bastian P et al. (2006) The Distributed and Unified Numerics Environment (DUNE) Grid Interface Proceedings of the 19th Symposium on Simulation Technique in Hannover

Bennett MH, Flemings PB, Hicks JR PJ, Shaw CA, Symington WA (1998) Simulation of secondary migration in faults: Dynamic Controls on hydrocarbon column height Aapg Bull 82 doi:10.1306/00AA868E-1730-11D7-8645000102C1865D

Bielinski A (2006) Numerical simulation of CO2 sequestration in geological formations Sprint-Druck, Stuttgart (Institute of Hydraulic Engineering, University of Stuttgart)

Buenz S, Tasianas A, Karstens J, Berndt C, Darcis M, Flemisch B (2012) Milestone Report (MS12): Geological models for industrial storage sites:103

Cartwright J, Huuse M, Aplin A (2007) Seal bypass systems Aapg Bull 91:1141-1166 doi:Doi 10.1306/04090705181

Cathles LM, Su Z, Chen DF (2010) The physics of gas chimney and pockmark formation, with implications for assessment of seafloor hazards and gas sequestration (vol 27, pg 82, 2010) Mar Petrol Geol 27:993-994 doi:DOI 10.1016/j.marpetgeo.2010.01.004

Chenevert ME, Sharma AK (1991) Permeability and effective pore pressure of shales SPE/IADC 21918

Darcis MY (2012) Coupling Models of Different Complexity for the Simulation of CO2 Storage in Deep Saline Aquifers. PhD thesis, Institut für Wasser- und Umweltsystemmodellierung, Universität Stuttgart

ECO2 (2014) Best Practice Guidance for Environmental Risk Assessment for offshore CO2 geological storage EU grant agreement no 265847. Deliverable 14.1

ECO2 (2015) ECO2 Final Publishable Summary Report http://wwweco2-projecteu/homehtml

Edlmann K, Edwards MA, Qiao XJ, Haszeldine RS, McDermott CI (2015) Appraisal of global CO2 storage opportunities using the geomechanical facies approach Environ Earth Sci 73:8075-8096 doi:10.1007/s12665-014-3965-3

Edlmann K, Haszeldine S, McDermott CI (2013) Experimental investigation into the sealing capability of naturally fractured shale caprocks to supercritical carbon dioxide flow Environ Earth Sci 70:3393-3409 doi:10.1007/s12665-013-2407-y

Eigestad GT, Dahle HK, Hellevang B, Riis F, Johansen WT, Oian E (2009) Geological modeling and simulation of CO2 injection in the Johansen formation Computat Geosci 13:435-450 doi:10.1007/s10596-009-9153-y

Eiken O, Ringrose P, Hermanrud C, Nazarian B, Torp TA, Hoier L (2011) Lessons Learned from 14 years of CCS Operations: Sleipner, In Salah and Snohvit Enrgy Proced 4:5541-5548 doi:DOI 10.1016/j.egypro.2011.02.541

Faleide JI et al. (2008) Structure and evolution of the continental margin off Norway and Barents Sea Episodes 31:82-91

Flemisch B et al. (2011) Dumux: Dune for multi-(Phase, Component, Scale, Physics, ...) flow and transport in porous media. Advances in Water Resources 34:1102-1112

Gabrielsen RH, Færseth RB, Jensen LN, Kalheim JE, Riis F (1990) Structural elements of the Norwegian Continental Shelf. Part 1: The Barents Sea region Norwegian Petroleum Directorate, Bulletin 6:33

Gonzalez-Nicolas A, Cody B, Bau D (2012) STOCHASTIC ANALYSIS OF FACTORS AFFECTING THE LEAKAGE OF CO2 FROM INJECTED GEOLOGICAL BASINS XIX International Conference on Water Resources CMWR 2012, University of Illinois at Urbana-Champaign, June 17-22, 2012

Green CP, Ennis-King J (2012) Spatial grid correction for short-term numerical simulation results of carbon dioxide dissolution in saline aquifers Computat Geosci 16:1153-1161 doi:DOI 10.1007/s10596-012-9309-z

Handy MR, Hirth G, Hovius N (2007) Tectonic faults : agents of change on a dynamic Earth. Dahlem Workshop reports, vol 95. MIT Press ;

In cooperation with the Freie Universität Berlin, Cambridge, Mass.Berlin

Hansen JØ, Rasen B (2012) Facts: The Norwegian Petroleum Sector Ministry of Petroleum and Energy and Norwegian Petroleum Directorate

Hansen O, Eiken O, Østmo S, Johansen RI, Smith A (2011) Monitoring CO_2 injection into a fluvial brine-filled sandstone formation at the Snøhvit field, Barents Sea. SEG San Antonio 2011 annual meeting

Helmig R (1997) Multiphase flow and transport processes in the subsurface - A Contribution to the the Modeling of Hydrosystems Springer-Verlag

House KZ, Schrag DP, Harvey CF, Lackner KS (2006) Permanent carbon dioxide storage in deep-sea sediments (vol 103, pg 12291, 2006) P Natl Acad Sci USA 103:14255-14255

Janssen C, Wirth R, Reinicke A, Rybacki E, Naumann R, Wenk HR, Dresen G (2011) Nanoscale porosity in SAFOD core samples (San Andreas Fault) Earth Planet Sc Lett 301:179-189 doi:DOI 10.1016/j.epsl.2010.10.040

Katsube TJ, Mudford BS, Best ME (1991) Petrophysical Characteristics of Shales from the Scotian Shelf Geophysics 56:1681-1689 doi:Doi 10.1190/1.1442980

Kim GY, Yi BY, Yoo DG, Ryu BJ, Riedel M (2011) Evidence of gas hydrate from downhole logging data in the Ulleung Basin, East Sea Mar Petrol Geol 28:1979-1985 doi:DOI 10.1016/j.marpetgeo.2011.01.011

Kissinger A, Noack V, Knopf S, Scheer D, Konrad W, Class H (2014) Characterization of reservoir conditions of CO_2 storage usting a dimensionless graviation number applied to the North German Basin Sustainable Energies, Technolgoies and Assessments, submitted

Ligtenberg JH (2005) Detection of fluid migration pathways in seismic data: implications for fault seal analysis Basin Res 17:141-153 doi:DOI 10.1111/j.1365-2117.2005.00258.x

Linjordet A, Olsen RG (1992) The Jurassic Snohvit Gas-Field, Hammerfest Basin, Offshore Northern Norway Aapg Memoir 54:349-370

Loseth H, Gading M, Wensaas L (2009) Hydrocarbon leakage interpreted on seismic data Mar Petrol Geol 26:1304-1319 doi:DOI 10.1016/j.marpetgeo.2008.09.008

Løtveit FI, Gudmundsson A, Sydnes M (2012) How the stress changes due to glacial erosion may have caused leakage of hydrocarbons in the SW Barents Sea Arctic Frontiers Conference Presentation

Makurat A, Torudbakken B, Monsen K, Rawlings C (1992) Cenozoic Uplift and Caprock Seal in the Barents Sea: Fracture Modelling and Seal Risk Evaluation. 1992/1/1/

Maldal T, Tappel IM (2004) CO_2 underground storage for Snohvit gas field development Energy 29:1403-1411 doi:DOI 10.1016/j.energy.2004.03.074

Meldahl P, Heggland R, Bril B, De Groot P (2001) Identifying faults and gas chimneys using multiattributes and neural networks Leading Edge 20:474-478

Mizoguchi K, Hirose T, Shimamoto T, Fukuyama E (2008) Internal structure and permeability of the Nojima fault, southwest Japan J Struct Geol 30:513-524 doi:DOI 10.1016/j.jsg.2007.12.002

Moore DE, Lockner DA, Ito H, Ikeda R, Tanaka H, Omura K (2009) Geometry of the Nojima Fault at Nojima-Hirabayashi, Japan - II. Microstructures and their Implications for Permeability and Strength Pure Appl Geophys 166:1669-1691 doi:DOI 10.1007/s00024-009-0513-2

Moumets H, Polivach Y, Zamora CS (2015) National Inventory Report - Snøhvit field 2014

Nordbotten JM, Celia MA (2012) Geological Storage of CO2: Modeling Approaches for Large-Scale Simulation John Wiley and Sons, New Jersey

Norden B, Forster A, Behrends K, Krause K, Stecken L, Meyer R (2012) Geological 3-D model of the larger Altensalzwedel area, Germany, for temperature prognosis and reservoir simulation Environ Earth Sci 67:511-526 doi:10.1007/s12665-012-1709-9

Opara AI (2011) ESTIMATION OF MULTIPLE SOURCES OF OVERPRESSURES USING VERTICAL EFFECTIVE STRESS APPROACH: CASE STUDY OF THE NIGER DELTA, NIGERIA Petroleum & Coal 53 (4):302-314

Ostanin I, Anka Z, di Primio R, Bernal A (2013) Hydrocarbon plumbing systems above the Snohvit gas field: Structural control and implications for thermogenic methane leakage in the Hammerfest Basin, SW Barents Sea Mar Petrol Geol 43:127-146 doi:DOI 10.1016/j.marpetgeo.2013.02.012

Ostanin I, Anka Z, Primio RD, Bernal A (2012) Identification of a large Upper Cretaceous polygonal fault network in the Hammerfest basin: Implications on the reactivation of regional faulting and gas leakage dynamics, SW Barents Sea. Marine Geology 332–334:109-125 doi:10.1016/j.margeo.2012.03.005

Ouakad HM, Nasrabadi H (2012) Onset of convection and advection in the CO2 sequestration-Problem using the lattice Boltzmann method International Journal of Advanced Science and Engineering Technology 2:68-75

Rodrigues Duran E, di Primio R, Anka Z, Stoddart D, Horsfield B (2013) Petroleum system analysis of the Hammerfest Basin (southwestern Barents Sea): Comparison of basin modelling and geochemical data Organic Geochemistry 63:105-121 doi:http://dx.doi.org/10.1016/j.orggeochem.2013.07.011

Schutze C et al. (2012) Natural analogues: a potential approach for developing reliable monitoring methods to understand subsurface CO2 migration processes Environ Earth Sci 67:411-423 doi:10.1007/s12665-012-1701-4

Van Oort E, Hale AH, Mody FK, Sanjit R (1996) Transport in shales and the design of improved waterbased shale drilling fluids SPE Drilling & Completion 11:137–146

Wibberley CAJ, Shipton ZK (2010) Fault zones: A complex issue J Struct Geol 32:1554-1556 doi:10.1016/j.jsg.2010.10.006

Worsley RJ, Edrich SP, Hutchison I (1988) The Mesozoic and Cenozoic succession of Tromsøflaket In: A Lithostratigraphic Scheme for the Mesozoic and Cenozoic Succession Offshore Mid- and Northern Norway Norwegian Petroleum Directorate Bulletin No. 4:42-65